

Impact of fracture properties on the performance of engineered geothermal systems in the crystalline basement of Kuujuaq (Canadian Shield)

Mafalda M. Miranda (✉ mafalda_alexandra.miranda@inrs.ca)

INRS – Institut national de la recherche scientifique

Jasmin Raymond

INRS – Institut national de la recherche scientifique

Chrystel Dezayes

BRGM – Bureau de Recherche Géologique et Minières

Andrew Wigston

CanmetENERGY-Ottawa, Natural Resources Canada

Serge Perreault

Centre d'études collégiales de Chibougamau

Research Article

Keywords: Petrothermal systems, photogrammetry, scanline, discrete fracture network, thermo-hydro-mechanical modeling, Nunavik

Posted Date: January 10th, 2023

DOI: <https://doi.org/10.21203/rs.3.rs-2416987/v1>

License:  This work is licensed under a Creative Commons Attribution 4.0 International License.

[Read Full License](#)

Abstract

Understanding the natural fracture network is essential for geothermal-related investigations. However, the geometrical attributes depend on the scale of observation. Therefore, a multiscale characterization of the fracture network is essential to ensure that forward heat and flow simulations are based on stochastically generated discrete fracture network models representative of the natural fracture system observed. This was the goal of this work. Fracture data was collected from satellite imagery, outcrops and well cores to evaluate the scale effect and to study the impact of fracture size and density on the performance of engineered geothermal systems by numerical modeling. The numerical simulations highlighted that networks made of small fractures (0.08 to 27 m) tend to decrease the performance of the system compared to a network made of large fractures (22 to 1,437 m). However, thermal short-circuiting is easily reached in the latter scenario. Thus, the simulations suggest that the best-case network is made of fractures ranging between 1.57 to 135 m with fractures spaced by 5 m. This scenario provides the best compromise between heat extraction, water losses, hydraulic impedance and thermal drawdown. Despite the uncertainties, the fracture data used highlights the importance of multiscale fracture analysis for heat-flow simulations of geothermal reservoirs.

Article Highlights

- A multiscale fracture network characterization using satellite imagery, outcrop and core data is presented.
- The scale effect of fracture properties on the performance of engineered geothermal systems is explored.
- Fracture size and spacing play an important role in the development of engineered geothermal energy systems.

1. Introduction

In Canada, over 280 communities are disconnected from the provincial/territorial power grid and primarily relying on diesel power plants for electricity and on oil furnaces for space heating and domestic hot water (CER, 2022). At the nowadays context where climate change and energy transition are buzzwords, many remote communities are exploring opportunities to reduce their reliance on fossil fuels, to improve energy security and to decrease the carbon footprint (CER, 2022). One of such opportunities include developing renewables (CER, 2022). In fact, a key component of the Government of Canada's Pan-Canadian Framework (GCan, 2022) is to reduce greenhouse gas emissions by helping remote communities transitioning from diesel-fired generation to cleaner energy sources. In this context, geothermal energy harnessed by deep technologies may be an alternative local option.

A geothermal system is mainly composed by a heat source, circulating fluids and permeability pathways at a drillable depth. However, the co-occurrence of geothermal heat and groundwater with sufficient

formation permeability is limited to few tectonically and volcanologically active locations around the globe (e.g., Moeck, 2014).

More common is the occurrence of deep formations that have enough heat potential but lack sufficient quantities of water and/or permeability. An example of such formations are low porosity crystalline rocks where permeability is mainly supported by a network of natural fractures that may be open or sealed. In instances where the natural fracture network exhibits poor hydraulic connection, its permeability needs to be increased to permit fluid circulation through the rock mass at rates of commercial interest. In this situation, the engineered/enhanced geothermal system (EGS) concept can be applied. This concept aims at enhancing well(s) productivity and formation permeability using hydraulic, chemical and/or thermal stimulation treatments, to engineer hydraulic linkages between two or more boreholes within the target reservoir, permitting circulation of fluid through the rock mass at rates of commercial interest (e.g., Genter et al., 2010). As a matter of fact, EGS could be an important technological advance to exploit geothermal energy sources from virtually anywhere in the world. For example, the application of EGS in Canada could not only permit the production of geothermal resources in unconventional geothermal plays, such as the Canadian Shield, but also enhance the production in conventional geothermal areas, such as the geothermal plays located in Canada's west coast. Ultimately, the development of EGS in Canada could help to decrease the diesel consumption in communities disconnected from the provincial/territorial power grids. However, the development of EGS technology faces many scientific and technical challenges (e.g., Pollack et al., 2021), one of those being related with reservoir development and circulation which is intimately related with the geometry and connectivity of the natural fracture network.

The major role played by the natural fracture network for the successful EGS development has been highlighted since the first EGS field experiments (e.g., Richards et al., 1994; Genter et al., 2010; Brown et al., 2012). The azimuth and dip of the fractures relative to the contemporary stress field determines which fractures will shear and at what fluid pressure. It also defines how the pressure-dilating region will develop and what the ultimate geometry of the reservoir will be. Furthermore, knowing the geometry of the fluid-conductive fractures is key to optimize the trajectories of the wells. Thus, the knowledge and characterization of the fracture network is of primary importance to exploit geothermal energy in crystalline fractured reservoirs, and it is not surprising that this task is undertaken at every geo-thermal site where EGS has been applied (e.g., Ledesert et al., 2010; Brown et al., 2012; Glaas et al., 2021; Reinecker et al., 2021).

However, the geometrical and topological attributes of fractures (i.e., orientation/azimuth, size/length, spacing, frequency and connectivity) are scale dependent (e.g., Hardebol et al., 2015; Espejel et al., 2020; Bossennec et al., 2021, 2022; Chabani et al., 2021a, b; Ceccato et al., 2022; Frey et al., 2022; Vega and Kovscek, 2022). For instance, well cores provide accurate subsurface information about azimuth, dip, spacing, frequency and aperture of fractures at a very narrow and local scale. Fracture size information, however, cannot be retrieved from well cores. Out-crop analogues, on the other hand, permit a wider local characterization of azimuth, dip, spacing, frequency, size, aperture and connectivity but are subject to censoring bias. Satellite imagery and LiDAR, for example, allow a regional investigation of the structural

lineaments (i.e., linear and curvilinear features that include geologic structures and geomorphologic features) in terms of azimuth, dip, spacing, frequency and connectivity and can better capture large-scale structural features such as lineament size. However, the information gathered by analyzing outcrop analogues, satellite imagery and LiDAR may not be representative of the deep-seated structures (e.g., Bauer et al., 2017). Therefore, a multiscale fracture network characterization should be undertaken to avoid misrepresentation and mischaracterization of fracture attributes.

Despite the scale effect is not a scientific novelty nowadays, with many publications highlighting the need for a multiscale fracture network characterization (e.g., Hardebol et al., 2015; Espejel et al., 2020; Bossennec et al., 2021, 2022; Chabani et al., 2021a, b; Ceccato et al., 2022; Frey et al., 2022; Vega and Kavscek, 2022), it is still an important issue to address when developing stochastic discrete fracture network (DFN) models for heat-flow simulations. Predicting EGS performance requires a stochastic DFN model that is illustrative of the natural fracture network observed, and multiscale datasets are helpful to obtain more representative fracture data.

The interest for a multiscale characterization increases when carrying out geo-thermal research in remote northern regions where typical geothermal exploration tools are often unavailable or need to be adapted to more affordable options – at least for a first-order evaluation of the deep geothermal potential. In remote northern regions, often, boreholes and cores are unavailable or are too shallow (< 300 m) to be illustrative of the deep-seated structures. Field campaigns in such remote areas are additionally expensive and limited in time. In this context, remote sensing techniques are helpful to analyze the target area in an affordable way. However, not all communities are covered by LiDAR and have visible outcrops for satellite imagery interpretation. Furthermore, the spatial resolution is a constraint. Thus, combining the different datasets seems to be a first-order solution to the problem.

In fact, access to an exhaustive dataset, allowing mapping at different scales in both surface (e.g., outcrop mapping, drone imagery, airborne LiDAR) and subsurface (e.g., cores, borehole, seismic), seems ideal to provide a comprehensive setting to fully characterize fracture networks and additional structural properties (e.g., Espejel et al., 2020). Thus, the objective of this study is to provide a first-order characterization of the geometrical attributes (orientation/azimuth, dip, size/length, spacing, density and aperture) of fractures using different datasets and study the impact of fracture size and density on the performance of an EGS.

2. Geology

2.1. Regional context

Kuujuuaq, the community studied to retrieve the fracture network information, is located on the Southeastern Churchill Province (SECP; Wardle et al., 1990, 2002; Wardle and van Kranendonk, 1996; James et al., 1996), a tectonic province of the Canadian Shield. The Canadian Shield is a large exposure

of Laurentia, the geologic core of the North American continent (e.g., Hoffman, 1988; Whitmeyer and Karlstrom, 2007; Hammer et al., 2010; Darbyshire et al., 2017).

The SECP consists of several lithotectonic blocks amalgamated during the Trans-Hudson Orogen (1.83–1.80 Ga; Corrigan et al., 2005, 2009; Whitmeyer and Karlstrom, 2007; Darbyshire et al., 2017; MERN, 2020) and is a rare example of a two-sided orogenic belt in which both flanks record transpressional development due to the oblique collisions that led to its assemblage (Wardle et al., 1990, 2002; Wardle and van Kranendonk, 1996).

Within the SECP, Kuujuaq is located on the Core Zone, the central portion between the Torngat Orogen (ca. 1.82–1.77 Ga; Wardle et al., 2002) and the New Quebec Orogen/Labrador Trough (ca. 1.82–1.77 Ga; Wardle et al., 2002). The latter suture involved whole-crustal shearing in the Core Zone and thin-skinned deformation in the New Quebec Orogen/Labrador Trough (Hall et al., 2002).

The Core Zone is a 35–40 km thick cratonic fragment mostly underlain by Archean tonalitic to granitic gneiss and granitoid rocks and is characterized by a pervasive E-dipping fabric related to westerly thrusting (James et al., 1996; Wardle et al., 2002; Corrigan et al., 2018). Within the Core Zone, Kuujuaq is located on the northern section of the Baleine lithotectonic domain (or Baie aux Feuilles domain; Simard et al., 2013). This section has also been termed Kuujuaq terrane (Perreault and Hynes, 1990) and Kuujuaq tectonic zone (Bardoux et al., 1998). In this area, the regional structural grain NW-SE to N-S observed resulted from the collision between the Core Zone and the Superior geological province (Fig. 1; Simard et al., 2013). The poles to plans of the main fabric observed in the domain delimited by Lac Gabriel and Lac Pingiajjulik faults are N338°E/30° (Fig. 1; Simard et al., 2013). Three main deformation phases (D1 to D3) have been identified in this region, corresponding to a continuous deformation process linked to the Labrador Trough development (Moorhead, 1989; Perreault and Hynes, 1990; Poirier et al., 1990; Goulet 1995; Simard et al., 2013). D1 and D2 phases are associated with the compression during collision of the cratons and D3 corresponds to the oblique component of the collision (Simard et al., 2013).

2.2. Local geology

Locally, two lithologies are dominant – paragneiss and diorite (Fig. 2). Smaller outcrops of gabbro, tonalite and granite are also observed (Fig. 2). The paragneiss belongs to the False Suite (Archean), the diorite is part of the Kaslac Complex (Paleoproterozoic), the gabbro is associated with the Ralleau Suite (Archean to Paleoproterozoic), the tonalite belongs to the Aveneau Suite (Paleoproterozoic) and the granite to the Dancelou Suite (Paleoproterozoic).

The following spatial and chronological arrangement description of the different geological units was proposed by Lafrance et al. (2020). The False Suite (3.3–2.7 Ga) is an extensive cover of Neoproterozoic metasedimentary rocks lying in discordance on top of the Archean gneiss bedrock formed by the Ungava Complex (2.7–2.9 Ga). The gneissic and migmatitic bedrock contain enclaves, levels and boudins of mafic and ultramafic intrusive rocks assigned to the Ralleau Suite. The intrusive units of the Kaslac

Complex (1.8 Ga) were emplaced within the gneisses of the Ungava Complex or the paragneisses of the False Suite. Rocks of the Kaslac Complex, located between the Lac Pingiajjulik and Lac Gabriel faults, have commonly undergone intense deformation characterized by the presence of mylonitic textures and quartz bands. The Aveneau Suite (1.8 Ga) is the largest Paleoproterozoic intrusive unit. Two different interpretations have been given to these rocks. Simard et al. (2013) interpreted them as partly representing the final fusion product of the gneisses of the Ungava Complex. Davis et al. (2015), on the other hand, proposed that this unit results either from crystallization that stretched over a long period of metamorphism or from the remobilization of slightly older Proterozoic rocks in association with an Archean component. The Aveneau Suite contains enclaves of the Ungava and Qurlutuq complexes and the Ralleau and False suites. Finally, the Dancelou Suite (1.7 Ga) represents the youngest Paleoproterozoic unit of the Baleine lithotectonic domain. It is made up of slightly deformed granitic intrusions that form well-circumscribed kilometric plutons scattered throughout the domain or that intruded in the form of dykes into older units. This unit also contains enclaves of surrounding units.

Two main regional faults cross the community. One of these structures is the Lac Pingiajjulik fault and the other is an unidentified fault. According to Poirier (1989), the Lac Pingiajjulik fault represents a large zone of highly recrystallized mylonite that separates two lithological blocks of different ages and is characterized by well-developed mylonitic foliation or banding. The Lac Pingiajjulik fault would be associated with an early NW-verging thrust phase, then folded during a subsequent deformation phase (Clark and Wares, 2004). Thus, the deformation of this fault is thrusting followed by late dextral movement (Perreault and Hynes, 1990). Rocks located to the east of the Lac Pingiajjulik fault are metamorphosed to the upper amphibolite facies and granulite facies. Rocks located to the west of this same structure are metamorphosed to the upper amphibolite facies. Strong recrystallization of mylonite indicates that metamorphic conditions were sufficient to allow static recrystallization after the main episode of deformation (Poirier et al., 1989). The Lac Pingiajjulik fault corresponds to a more or less sharp lineament that follows the contour of lithodemic units on the regional aeromagnetic map (MERN, 2020). Furthermore, the Lac Pingiajjulik fault is masked in several places by Paleoproterozoic intrusive rocks of the Aveneau and Dancelou suites, suggesting that the fault predates the emplacement of these intrusive units. Near the community of Kuujuaq, the presence of the Lac Pingiajjulik fault is given by the mylonitic foliation parallel to the fault trace on the geological map (Fig. 3).

2.3. Description of the datasets

Structural lineaments were analyzed by interpretation of Google Earth satellite images and fracture information (i.e., azimuth, dip, length, spacing, frequency, aperture and connectivity) was collected in outcrops and well cores.

2.3.1. Satellite imagery

The satellite imagery for interpretation of the structural lineaments was retrieved from Google Earth (Fig. 4). The outcrop analyzed is located on the east side of the Koksoak River and it is made mostly of

gneissic rocks of the Ungava Complex (see Fig. 2 for geographical location). A total of 226 structural lineaments were interpreted, suggesting an aerial frequency of 13.29 km^{-2} . Interpretation of the structural lineaments suggests a main lineament orientation E-W and NE-SW (Fig. 4).

2.3.2. Outcrops

Six sampling areas were selected to carry out fracture analysis (A1 to A6; see Fig. 2 for geographical location). Sampling area 1 (A1) is located near the Coop store in Kuujjuaq (Fig. 5). In this area, a total of 6 outcrops were analyzed (Appendix A). Sampling area 2 (A2) is located outside of the community in an area informally called Trois lacs (Fig. 5). In this area, 5 outcrops were investigated (Appendix A). Sampling area 3 (A3) is located within the community, near a new treatment center and Koksoak River (Fig. 5). In this area, fracture data was collected in 8 outcrops (Appendix A). Sampling area 4 (A4) is located near the Hydro-Quebec diesel power plant (Fig. 5). In this area, 3 outcrops were analyzed (Appendix A). Sampling area 5 (A5) is located near the graveyard (Fig. 5). In this area, fracture data was sampled in 3 outcrops (Appendix A). Sampling area 6 (A6) is located near the dock (Fig. 5). This is the only outcrop with a vertical surface.

The outcrops in sampling areas A1 and A2 are made of paragneiss rocks from the False Suite and the outcrops in A3 and A4 are made of diorite rocks from the Kaslac Complex. The outcrops in sampling area A5 are near the contact between the paragneiss rocks of False Suite and tonalite rocks of Aveneau Suite and both rocks were observed. Sampling area A6 corresponds to the contact between gabbro rocks from the Ralleau Suite and tonalite rocks from the Aveneau Suite.

2.3.3. Core

The core recovered from a near 240 m deep well drilled near the Forum building in Kuujjuaq (see Fig. 2 for geographical location) was analyzed in terms of lithology and structures (Fig. 6). The main lithology encountered was paragneiss rocks from the False Suite, interlayered with diorite and gabbro rocks from Kaslac Complex and Ralleau Suite and granitoid rocks from the Kaslac Complex and Aveneau and Dancelou suites. A total of 187 possible natural fractures were interpreted, suggesting a linear fracture frequency of 0.80 m^{-1} and a mean apparent fracture spacing of 1.11 m. The interpretation took into consideration the shape of the fractures and the mineralization. The core was not oriented and neither borehole images were taken (e.g., borehole televiewer) and therefore information about fracture orientation and dip was not retrieved. Further information about the geological core logging is given by Miranda and Raymond (2022). The interpretation of the well core neither suggests a relationship between lithology and fracture frequency nor between fracture frequency and depth (Fig. 6).

3. Methods And Techniques

3.1. Fracture data collection and analysis

3.1.1. Satellite imagery

The satellite image was retrieved from Google Earth and interpreted in ArcGIS version 10.3 using the Editor – straight element function to manually depict the structural lineaments. Then, trace direction and size were evaluated as explained in the ESRI technical support webpage – How to: Batch calculate line direction using the Field Calculator (ESRI, 2021). The information gathered about trace orientation was then used in Grapher (Golden Software, 2022) to produce the rose diagram.

Probability distribution functions (PDFs) were applied to characterize the trace orientation and size (Appendix B) and statistical tests such as the root mean squared error (RMSE) and the sum of squared errors (SSE) were used to evaluate which PDF best fit the data sampled (Appendix C) as suggested by Zeeb et al. (2013b).

3.1.2. Outcrops

The linear scanline sampling method together with a transit compass corrected for the magnetic declination (22° in Kuujuaq) and an electronic caliper were used to collect fracture geometrical attributes (i.e., azimuth, dip, size and aperture) and the position of fractures along the scanline. A total of 1 to 4 scanlines per outcrop were used in an attempt to fully characterize the outcrop surface.

Grapher (Golden Software, 2022) was used to build the rose diagrams considering the azimuths of the fractures observed and Stereonet version 11.3.7 (Allmendinger, 2021) to produce stereonet canvas. PDFs were applied to characterize the fracture orientation, size, spacing and aperture (Appendix B). Then, statistical tests such as the RMSE and the SSE were used to evaluate which PDF best fit the data sampled (Appendix C) as suggested by Zeeb et al. (2013b).

3.1.3. Core

The linear scanline sampling method was also used to locate the structures along the well core and obtain information about fracture frequency and spacing. The tape was placed parallel to the core length and thus vertical structures are underrepresented since these are parallel to the scanline. PDFs were applied to characterize the data gathered (Appendix B) and statistical tests were used to evaluate which PDF best fit the data sampled (Appendix C) as suggested by Zeeb et al. (2013b).

3.2. Numerical simulations

The numerical simulations were carried out with FRACSIM3D (Jing et al., 2000; Miranda et al., 2021), a fracture generator and thermo-hydro and hydro-mechanical coupled model. FRACSIM3D generates a stochastic fracture network following a conventional Poisson model. Fractures are uniformly spaced and randomly located within the specified model volume (8 km³ in this case). The fracture size is assumed to be fractal. After the fracture generation process is finished, FRACSIM3D simulates the hydro-mechanical coupled process of reservoir development through hydraulic stimulation or hydroshearing. Then, FRACSIM3D finally simulates the thermo-hydro coupled process of circulation and heat extraction. It is important to highlight that the flow within the model is dependent on how well the fractures slip, which is

dependent on the mechanical properties assumed for the medium and the stimulation volume and fluid pressure defined, and the pressure at which the wells are held during circulation.

A cubic model volume of 8 km^3 (with 2 km of edge length) discretized into a grid of $200 \times 200 \times 200$ cells was used to carry out the numerical simulations. A grid dependency study was undertaken and revealed a difference of about 5% between a 100-cell grid and a 300-cell grid. The system was designed as a doublet, with one injector and one producer, both assumed vertical. A spacing of 600 m was assumed between the wells and an open hole length of 600 m was considered. The wells were positioned oriented parallel to the maximum horizontal principal stress. The well bore radius was defined as 0.11 m. A stimulation pressure of 12 MPa km^{-1} and a stimulation volume of 0.8 km^3 was assumed for both wells, which were held at a pressure of 14 MPa (injector) and - 2 MPa (producer) during circulation. Assumptions for the properties of the medium are taken from Miranda et al. (2021; Table 1). The simulations were run for a period of 20 years.

Table 1

Medium properties assumed as input parameters for simulations (Miranda et al., 2021).

Parameter	Symbol	Unit	Value
Maximum horizontal principal stress	σ_H	MPa km ⁻¹	45.3
Direction maximum horizontal principal stress	σ_H	°	N215°E
Minimum horizontal principal stress	σ_h	MPa km ⁻¹	26.5
Direction minimum principal stress	σ_h	°	N305°E
Vertical principal stress	σ_V	MPa km ⁻¹	27
In situ fluid pressure	P_{pore}	MPa km ⁻¹	10.8
In situ fluid density	ρ_{fluid}	kg m ⁻³	1080
In situ fluid dynamic viscosity	w	kg m ⁻¹ s ⁻¹	3.19×10^{-4}
Temperature	T	°C km ⁻¹	22
Permeability	k	m ²	10^{-17}
Thermal conductivity	λ_{rock}	W m ⁻¹ K ⁻¹	2.0
Volumetric heat capacity	ρC_{rock}	MJ m ⁻³ K ⁻¹	2.4
Young's modulus	E	GPa	71.5
Poisson's ratio	ν	—	0.23
Asperity strength factor	F_{asperity}	—	0.5
Basic friction angle	Φ_{basic}	°	24.5
Initial shear dilation angle	$\Phi_{\text{dilation},0}$	°	2.5
Peak shear dilation angle	$\Phi_{\text{dilation,peak}}$	°	10.0
Post-peak shear dilation angle	$\Phi_{\text{dilation,post-peak}}$	°	5.0
Peak shear displacement	U_{peak}	mm	5.0
Post-peak shear displacement	$U_{\text{post-peak}}$	mm	2.5
Reference stress for 90% closure	$\sigma_{n,\text{ref}}$	MPa	50
Re-injection temperature	$T_{\text{injection}}$	°C	30

Parameter	Symbol	Unit	Value
Circulation fluid density	ρ_{fluid}	kg m ⁻³	993
Circulation fluid specific heat	c_{fluid}	J kg ⁻¹ K ⁻¹	4180

4. Results

4.1. Fracture data analysis

The structural lineaments and fracture data collected from the satellite image, outcrops and well core were analyzed separately and combined to answer the following research questions:

- 1) How does the scale of observation influence the geometrical attributes of fracture networks on crystalline rocks?
- 2) Which probability distribution function (PDF) to characterize geometrical fracture attributes best fits the data collected?

The Mixture of von Mises (MvM) distributions with 18 elements suggests a multimodal orientation indicating five main families (Fig. 7): F1 – N81-90°E (E-W), F2 – N41-50°E (NE-SW), F3 – N101-110°E (NW-SE), F4 – N21-30°E (NNE-SSW) and F5 – N151-160°E (NNW-SSE).

Analysis of the size suggest that 50% of the interpreted structures in the satellite image are below 300 m, while 50% of outcrop fractures are below 2 m (Fig. 7). Combining both datasets suggest that the DFN would be characterized by 65% of structures below 50 m and 35% of structures between 50 to 1,437 m. More specifically, a DFN generated with these datasets would have 50% of the structures smaller than 3 m, 35% of the structures larger than 100 m and 15% of the structures between 3 and 100 m. This highlights the greater number of small fractures observed compared to larger structures, agreeing with the fact that a power-law distribution provides the best fit to the structures size. The RMSE for the power-law distribution was evaluated to be 0.25, while for the exponential and lognormal distribution was 0.29 and 0.35, respectively. The SSE for the power-law distribution was estimated to be 40, while for the exponential and lognormal distribution was 52 and 80, respectively.

As the power-law distribution best describes the fracture sizes, it can be assumed that the network follows a fractal size distribution. The power-law exponent, or fractal dimension, considering the whole untruncated dataset is -0.3. However, application of the chord method suggests a lower cutoff fracture size of 200 m and a power-law exponent of -2.1. The chord method is based on the log-log plot of fracture size against cumulative frequency. A line is drawn through the data point with the shortest length and the data point with the longest length. Then, the data point with the longest perpendicular distance from this line is used as the lower cutoff (Zeeb et al., 2013a).

Spacing data interpreted suggest that the best fit is given by an exponential dis-tribution, which indicates a uniform spatial distribution for the structures (Fig. 7). The RMSE for the exponential distribution is 0.06 and the SSE is 2. The power-law distribution, on the other hand, revealed RMSE and SSE of 0.56 and 159. Furthermore, analysis of the data indicates that the core has more widely spaced fractures than the outcrops. Average fracture spacing obtained from the core data is 1.11 m while out-crop average fracture spacing is 0.55 m. This agrees with the linear fracture frequency estimated. Core data revealed a value of 0.80 m^{-1} while outcrop data suggest an average value of 1.81 m^{-1} . In other words, while core data indicates less than a fracture per meter of core, outcrop data implies almost 2 fractures per meter of outcrop.

Fracture aperture measured in the field with an electronic caliper indicates a mean value of 6.5 mm, with a minimum value of 0.1 mm and a maximum value of 165 mm (Fig. 7). These values indicates that the apertures range from tight to wide, but with different probability of occurrence (Table 2). It is important to highlight, however, that these apertures are greatly influenced by weathering of the fracture walls and may not correspond to the in situ aperture value. The data collected also suggests that a power-law distribution has the best fit, with a RMSE of 0.17 and a SSE of 9. A lognormal distribution reveals a RMSE of 0.29 and a SSE of 27.

Table 2
Aperture classification (ISRM, 1978) and probability of occurrence.

Aperture (mm)	Classification	Probability (%)
< 0.1	Very tight	0
0.1–0.25	Tight	25
0.25–0.50	Partly open	4
0.50–2.50	Open	38
2.50–10.0	Moderately wide	23
> 10.0	Wide	11

Additionally, the outcrop data from sampling areas A1, A2, A3 and A4 was analyzed to understand if lithology influences the geometrical attributes of fractures, thus answering to the following research question:

3) How does lithology influence the geometrical attributes of fractures?

The results suggest that the paragneiss rocks have three main fracture sets given by the MvM distributions (Fig. 8): F1 – N81-90°E (E-W), F2 – N151-160°E (NW-SE) and F3 – N1-10°E (N-S). Three

main fracture families were also identified for the diorite rocks which are (Fig. 8): F1 – N91-100°E (E-W), F2 – N121-130°E (NW-SE) and F3 – N151-160°E and N161-170°E (NNW-SSE). These results seem to suggest that, despite the different distribution of values, both lithologies have the same fracture sets.

Fracture size is also similar for both paragneiss and diorite (Fig. 8). These lithologies revealed a median fracture size of 1.4 m and 2 m, respectively for paragneiss and diorite. However, the diorite rocks have a larger dispersion of fracture size than paragneiss rocks.

Similarly, minimal differences were also found for fracture spacing (Fig. 8), with the paragneiss revealing a mean fracture spacing of 0.18 m and the diorite 0.36 m, with the latter showing larger data dispersion. Aperture data also reveals minimal differences (Fig. 8), with both paragneiss and diorite revealing the same median aperture of 1.5 mm and similar data dispersion.

4.2. Numerical simulations

Numerical simulations were carried out to answer the last research question:

4) What are the implications of this study for EGS development?

Nine scenarios were simulated to answer this question by changing the fracture size and frequency but keeping the fracture orientation constant (Table 3). For the structural lineaments extracted from the satellite image, a slip patch radius of 150 m was assumed as a working hypothesis and to prevent unrealistic flow rates. In scenario 2C, the pressure at which the wells are held during circulation was modified to 30 MPa (injector) and -20 MPa (producer) and in scenario 2D the stimulation pressure in both wells was increased to 51 MPa. Scenario 3A corresponds to the untruncated fracture size while scenarios 3B and 3C were built considering the fracture size within the 30–70% interval.

Table 3
Numerical simulation scenarios.

Scenario	Input	Output						
	Fracture orientation	l (m)	S (m)	$Q_{\text{recovered}}$ (l s ⁻¹)	W_{loss} (%)	l (MPa L ⁻¹ s ⁻¹)	T_{drawdown} (°C/year)	$P_{\text{recovered}}$ (GWh/year)
1A	Outcrop	22 to 1,437	10	51	26	0.3	1.3	86
1B	Outcrop	22 to 1,437	5	75	2	0.2	1.0	125
2A	Outcrop	0.08 to 28	5	0.7	65	22.9	—	—
2B	Outcrop	0.08 to 28	1.11	6	52	2.7	0.1	12
2C	Outcrop	0.08 to 28	1.11	22	45	2.3	0.1	45
2D	Outcrop	0.08 to 28	1.11	56	34	0.9	0.2	115
3A	Outcrop	0.08 to 1,437	3.3	44	71	0.4	1.0	88
3B	Outcrop	1.57 to 135	10	18	49	0.9	0.9	35
3C	Outcrop	1.57 to 135	5	48	29	0.3	0.7	95

l – fracture size, S – fracture spacing, $Q_{\text{recovered}}$ – flow rate, W_{loss} – water loss, l – hydraulic impedance, T_{drawdown} – temperature drawdown, $P_{\text{recovered}}$ – thermal output.

The simulations suggest that a network made exclusively of small fractures (Scenario 2A – 2C) leads to a greater reservoir impedance and lower heat extraction compared to a network made exclusively of large fractures (Scenario 1A – 1B and 3A – 3C; Fig. 9). However, a network of large fractures may lead to an early thermal short-circuiting of the reservoir, as only a handful of fractures will be conducting flow (Scenario 1A; Fig. 9). Nevertheless, this behavior changes if the density of the network is increased (Scenario 1B; Fig. 9), or if smaller fractures are introduced in the network (Scenario 3A – 3C; Fig. 9). An interesting point illustrated by the simulations undertaken is that a network made of small fractures will need greater fracture density to achieve the same flow rates as a network made of larger fractures. Water losses are also decreased in a network with greater fracture density. Furthermore, a network made exclusively of small fractures tends to be more productive with greater fluid stimulation and circulation pressures.

One of the causes for the different EGS performances may be related with the fracture shear stiffness. This parameter is approximated in FRACSIM3D as the ratio of the rock shear modulus divided by the fracture radius and multiplied by a geometric parameter (Dieterich, 1957; Eshelby, 1978; Willis-Richards et al., 1996). For the same shear modulus, a fracture with 0.08 m has a shear stiffness of about 333 GPa m⁻¹ while a 1,437 m fracture has 0.02 GPa m⁻¹ of shear stiffness. The lowest shear stiffness values are thus found for the fracture network made of large fractures (e.g., Scenario 1A) while the greatest values for the fracture network made of small fractures (e.g., Scenario 2B).

Additionally, the capacity of the EGS simulated to fulfil the heating demand of Kuujuaq was investigated. The annual average heating needs of a typical residential dwelling in Kuujuaq have been evaluated to be 22 to 71 MWh (Yan et al., 2019; Gunawan et al., 2020). This community has 973 dwellings, implying an annual average heating demand of 21 to 69 GWh. Furthermore, an annual population growth of 3% has been noticed through Census. Thus, assuming the same growth rate in heating demand, in 20 years, the annual average heating demand of this community may be 38 to 121 GWh. Keeping these values in mind, the simulation results indicate that Scenario 1A, 1B, 2C, 2D, 3A and 3C are able to fulfil the demand over the lifespan of the system considering the lower bound of demand (Table 3). However, these conclusions change considering the upper bound of heating demand. In this case, only Scenario 1B has sufficient thermal extraction to fulfil the heating demand (Table 3). However, the best compromise between heat extraction, water losses, reservoir hydraulic impedance and thermal drawdown is given by Scenario 3C, where a mix between small and large fractures spaced by 5 m was considered.

5. Discussion

Renewable energy technologies can be a catalyst for the sustainable development of Canada's north, if Indigenous Peoples are interested in deploying them. Thus, many scholars have been focusing their research on finding the optimal renewable technology and design to meet the power and heating needs of Indigenous communities in the context of affordability, environmental compatibility, reliability and ease of use/repair (e.g., Ranjitkar et al., 2006; Thompson and Duggirala, 2009; Kunkel et al., 2012; Walsh, 2013; Majorowicz and Grasby, 2014; Majorowicz and Minea, 2015; Stephen et al., 2016; McFarlan, 2018; Giordano and Raymond, 2019; Kanzari, 2019; Yan et al., 2019; Gunawan et al., 2020; Mahbaz et al., 2020; Qitoras 2020).

Earth energy sources harnessed by deep geothermal technologies may be one of several viable options for remote northern communities. The versatility of geothermal energy places it in a privileged position since in northern regions most of energy consumed is for space heating. However, despite the potential benefits, geothermal energy is still seen as a high-risk option in Canada since data gaps limit assessment to only about 40% of the country's landmass (Grasby et al., 2012). In fact, the Canadian Shield has been seen as a low potential and unviable area for geothermal production due to the low geothermal gradient and low permeability of the Archean and Paleoproterozoic rocks that constitute the Shield. However, emerging concepts such as EGS may be able to make this productive less area into a target region. This, ultimately, can be a valuable contribution to the energy transition of remote northern communities.

However, prior to assessing EGS performance, it is important to understand the deep-seated structures that can act as flow pathways. One way of acquiring such knowledge is by collecting fracture geometrical data (i.e., azimuth, dip, size, spacing, frequency, aperture) from exposures of rock outcrops and boreholes, quarries, tunnels and roadcuts (e.g., Lei et al., 2017). This data can be sampled using linear and circular scanlines and rectangular window methods (Zeeb et al., 2013a; Watkins et al., 2015). Beyond these, areal sampling using photogrammetry (outcrop aerial photographs, satellite imagery) and virtual outcrop methods (DEM, LiDAR) are nowadays widely applied (e.g., (Fisher et al., 2014; Cawood et al., 2017; Salvini et al., 2017; Chapelet et al., 2020; Binda et al., 2021; Colica et al., 2021; Kong et al., 2021)). In fact, the combination of these different sampling methods allows a multiscale analysis for a full characterization of the fracture network avoiding misrepresentation and mischaracterization of the structures (e.g., Hardebol et al., 2015; Espejel et al., 2020; Bossennec et al., 2021, 2022; Chabani et al., 2021a, b; Ceccato et al., 2022; Frey et al., 2022).

Espejel et al. (2020), for instance, observed that both geometrical and topological fracture attributes are scale dependent. Furthermore, these authors recognised transitional scale gaps of fracture size between different scales of observation which greatly constrains the fracture network characterisation. This transitional fracture scale gap is also observed with different fracture sizes in this study. While outcrop analysis suggests fractures with sizes ranging between 0.08 to 27 m, with the majority of structures smaller than 5 m, the interpretation of satellite imagery suggests structural lineaments ranging from 22 to 1,437 m. This size difference caused by the scale of observation has an impact on EGS performance as highlight in our study. On one hand, hydraulic stimulation treatments may be less effective when applied to a network made exclusively of small size fractures. Small size fractures tend to slip less making fluid circulation more difficult through those structures. However, on the other hand, a network made exclusively of large size fractures can lead to an early short-circuiting of the system, with only a few fractures acting as flow pathways.

Bossennec et al. (2021), Chabani et al. (2021a) and Ceccato et al. (2022) were able to fit their fracture size derived from different datasets to a global power law with an exponent of about -2. This means that a homogeneous value could be used for different DFN modelling scales and that connectivity is ruled by the small and the large fractures. The results of our study, however, suggests two different power law exponents. The power law exponent for the structural lineaments interpreted from satellite imagery is -1.2 and the power law exponent for the fractures observed at the outcrop scale is -0.95. Nevertheless, combining both datasets leads to a power law exponent of -0.3, or -2.1 if the chord method is applied. These results highlight the large number of small size fractures observed in this study compared to large fractures, and that connectivity is mostly ruled by the small size fractures.

Bossennec et al. (2021) and Ceccato et al. (2022) also observed that fracture orientation is dependent of the scale of observation. In their study, the regional directions observed are not expressed with the same proportion at all scales. Similar observation was made in our study. While the fracture analysis at the outcrop scale suggests a main fracture family, the interpretation of the satellite image suggest more heterogeneity of fracture directions, with five main families. These results suggest that the outcrop as a

preferential permeability orientation while the permeability derived from structural lineaments observed at the satellite imagery scale is more heterogeneous, without a preferential direction, and therefore a homogeneous value could be a first-order approximation to simplify numerical modeling. Nevertheless, as fracture orientation contributes significantly to directional permeability, this fracture property should be properly studied. In our study, a MvM distributions with 18 components was used to characterize fracture orientation. However, this can be further improved by application of “BAMBI” R software package and the Python code described by Chabani et al. (2020). Furthermore, the approach described by Tran (2007) can be further applied to characterize fracture orientation and minimize statistical errors that can have an important impact on numerical models.

Ceccato et al. (2022) observed that spatial distribution was scale-invariant for their different datasets. In our study, however, the scale effect on fracture spacing and linear frequency is less significant than on orientation and size, but still exists. Furthermore, while Ceccato et al. (2022) observed that lineament size, density, and intensity distributions each follow scaling power-law, our fracture data suggests otherwise. Fracture size follows a power-law distribution, but an exponential distribution provides a better fit to the spatial fracture distribution. The choice of the appropriate PDF is in fact an important step when analyzing fracture data. Hamzehpour et al. (2021) studied the impact of PDFs to characterize fracture attributes on percolation and flow properties. Their observations suggest that the PDF chosen has an important impact on the permeability and porosity of fracture networks and thus the PDF that best suits the data is an important aspect to consider. Future improvements to the statistical analysis can be made by following the approach of Guerriero et al. (2011).

Another important aspect studied in this work was the influence of lithology on the geometrical properties of fractures. The data collected revealed that fracture orientation, size, spacing and aperture can be considered independent of lithology. This has important consequences for further numerical modeling. Since the geometrical attributes are independent of lithology, the DFN model can be simplified, grouping information from both main lithologies encountered. A similar observation has been made by Chapman et al. (submitted), who analyzed fracture data in SW Yukon at the outcrop scale and did not recognize a correlation between lithology and fracture attributes.

Glaas et al. (2021) present a structural characterization of the naturally fractured geothermal reservoirs in the central Upper Rhine Graben. Their results suggest that the average fracture density in the granitic basement can range between 0.36 and 1.60 fractures per meter, with the well ESP-1 showing high fracture density, with an average value of 3.85 fractures per meter. The core recovered from the Forum well suggests an average fracture density similar to the one observed by Glaas et al. (2021) in the Upper Rhine Graben. The Upper Rhine Graben is a geothermal productive area, where the geothermal reservoirs are associated with the naturally fractured granitic basement. The fact that similar fracture densities were observed in our study reinforces the hypothesis that the Canadian Shield beneath Kuujuaq may be a potential area for geothermal developments.

Furthermore, the high density of fractures observed at the outcrop and core scales may indicate that the fracture network could be approximated as an equivalent porous media for heat-flow simulations. Equivalent porous media can help to reduce the computational cost and model complexity. However, Zareidarmiyani et al. (2021) observed that despite equivalent porous media are capable to reproduce pressure and temperature evolution at wells, it fails at reproducing the distributions within the fractured media. Thus, the equivalent porous media approach should be used with care, and under some circumstances, this approach cannot substitute the numerical simulations using DFN models.

The fracture data analysis undertaken in this study provides the essential information to produce computational representations (i.e., stochastic DFNs) that are representative of the natural fracture network for thermal, hydraulic and mechanical simulations. Furthermore, it also offers important observations for EGS development in Kuujuaq, a remote community located in Canada and heavily relying on diesel that can be a potential target for geothermal energy production using EGS concept. The multiscale fracture network characterization, using satellite images, outcrops and well cores, suggests that the effectiveness of hydraulic stimulation depends on the fracture size and spacing. Reservoirs of potential commercial interest can be achieved if the connectivity of the network is ruled by both small and large size fractures and if these are closely spaced.

6. Conclusions

Despite the scale effect being known, it is still a challenging aspect to consider when analyzing fracture data with the goal of generating stochastic DFNs and understand the deep-seated structures.

The results of this work highlight that orientation, size and connectivity are greatly dependent on the scale of observation. Despite existent, the scale effect on fracture spacing and linear frequency is less significant. Outcrop data alone suggest one main fracture set while the combination of satellite image and outcrop data indicates five main families. Furthermore, outcrop data indicates fractures smaller than 30 m while structural lineaments of up to near 1,500 m were identified in the satellite image. A power-law distribution provides the best fit for the fracture size. Additionally, core data reveals more widely spaced fractures, and consequently lower linear fracture frequency, than outcrop data. The data also suggests that fracture spacing can be fit to an exponential distribution. Fracture aperture is found to obey a power-law distribution. Finally, connectivity analysis suggests that the small-scale outcrops tend to have greater connectivity than large scale (i.e., satellite imagery scale) outcrops.

The numerical simulations of EGS performance suggest that a network composed by larger fractures (satellite imagery size; 22 to 1,437 m) performs better than a network composed by smaller fractures (outcrop size; 0.08 to 28 m). One reason is the lower shear stiffness of larger fractures. However, a network made exclusively of larger fractures tend to increase the probability of reservoir thermal short-circuiting. The simulations also illustrate that a small fracture size network needs greater fracture frequency and/or greater stimulation and circulation pressures to achieve similar flow rates to a large fracture size network.

Despite being a case study, the work described here aims at acquiring new knowledge on the geometry and connectivity of natural fracture networks. This is essential to proceed with exploration steps and evaluate the technical feasibility of EGS in Precambrian basement rocks. This represents a valuable contribution for the geo-thermal community assessing the potential of geothermal technologies in northern environments and dealing with important data gaps. However, the authors are well aware that deep geothermal exploration boreholes are needed to validate any estimates based on outcrop analogues. Nevertheless, to raise the interest for geothermal exploration drilling, research needs to be undertaken using data that can be economically collected. This is where this contribution gains its scientific value.

Declarations

Acknowledgments: The Centre d'études nordiques (CEN), supported by the Fonds de recherche du Québec – nature et technologies (FRQNT), and the Observatoire Homme Milieu Nunavik (OHMI) are acknowledged for helping with field campaigns and logistics. The authors are also thankful to Cynthia Brind'Amour-Cote for the support during the field campaign and to Jonathan Willis-Richards who provided the code FRACSIM3D used to run the EGS numerical simulations.

Ethics Approval: Not applicable.

Conflict of Interest: The authors declare no conflict of interest.

Data Availability Statement: All the data is presented in the manuscript.

Author Contributions: Conceptualization, M.M.M. and C.D.; methodology, M.M.M., J.R. and C.D.; validation, M.M.M., J.R., C.D., A.W. and S.P.; formal analysis, M.M.M.; investigation, M.M.M.; resources, M.M.M.; data curation, M.M.M.; writing—original draft preparation, M.M.M., J.R., C.D., A.W. and S.P.; writing—review and editing, M.M.M., J.R., C.D., A.W. and S.P.; visualization, M.M.M.; supervision, J.R.; project administration, J.R.; funding acquisition, J.R. All authors have read and agreed to the published version of the manuscript.

Funding: This research was funded by the Institut nordique du québec (INQ) through the Chaire de recherche sur le potentiel géothermique du Nord awarded to Jasmin Raymond and by Natural Resources Canada.

Consent to publish: The authors agree with the publication of the manuscript.

References

1. Allmendinger RW (2020) Stereonet v. 11. <https://www.rickallmendinger.net/stereonet>. Accessed on 09 September 2022.

2. Bardoux M, Digonnet S, Donohue L, Giard B, Robillard M, David J, Parent M, Gariépy C (1998) Paleoproterozoic tectonics affecting Archean lower crust of southern Ungava Bay. In Eastern Canadian Shield Onshore–Offshore Transect (ECSOOT), Report of the 1998 Transect Meeting; Wardle, R.J., Hall, J., Eds.; University of British Columbia: Vancouver (BC), Canada; Report 68, pp. 1-17.
3. Bauer JF, Krumbholz M, Meier S, Tanner DC (2017) Predictability of properties of a fractured geothermal reservoir: the opportunities and limitations of an outcrop analogue study. *Geothermal Energy* 5:24. <https://doi.org/10.1186/s40517-017-0081-0>
4. Binda G, Pozzi A, Spanu D, Livio F, Trotta S, Bitonte R (2021) Integration of photogrammetry from unmanned aerial vehicles, field measurements and discrete fracture network modeling to understand groundwater flow in remote settings: test and comparison with geochemical markers in an Alpine catchment. *Hydrogeology Journal* 29:1203-1218. <https://doi.org/10.1007/s10040-021-02304-4>
5. Borradaile G (2003) *Statistics of Earth Science Data*. Springer, Heidelberg, Germany
6. Bossennec C, Frey M, Seib L, Bär K, Sass I (2021) Multiscale characterisation of fracture patterns of a crystalline reservoir analogue. *Geosciences* 11:371. <https://doi.org/10.3390/geosciences11090371>
7. Bossennec C, Seib L, Frey M, van der Vaart J, Sass I (2022) Structural architecture and permeability patterns of crystalline reservoir rocks in the Northern Upper Rhine Graben: Insights from surface analogues of the Odenwald. *Energies* 15:1310. <https://doi.org/10.3390/en15041310>
8. Brown DW, Duchane DV, Heiken G, Hrisco VT (2012) *Mining the Earth's Heat: Hot Dry Rock Geothermal Energy*. Springer, Heidelberg
9. Cawood AJ, Bond CE, Howell JA, Butler RWH, Totake Y (2017) LiDAR, UAV or compass-clinometer? Accuracy, coverage and the effects on structural models. *Journal of Structural Geology* 98:67-82. <https://doi.org/10.1016/j.jsg.2017.04.004>
10. Ceccato A, Tartaglia G, Antonellini M, Viola G (2022) Multiscale lineament analysis and permeability heterogeneity of fractured crystalline basement blocks. *EGUsphere*. <https://doi.org/10.5194/egusphere-2022-255>
11. CER (2022) Market Snapshot: Overcoming the challenges of powering Canada's off-grid communities. <https://www.cer-rec.gc.ca/en/data-analysis/energy-markets/market-snapshots/2018/market-snapshot-overcoming-challenges-powering-canadas-off-grid-communities.html>. Accessed on 07 September 2022
12. Chabani A, Mehl C, Cojan I, Alais R, Bruel D (2020) Semi-automated component identification of a complex fracture network using a mixture of von Mises distributions: Application to the Ardeche margin (South-East France). *Computers & Geosciences* 137:104435. <https://doi.org/10.1016/j.cageo.2020.104435>
13. Chabani A, Trullenque G, Ledésert BA, Klee J (2021a) Multiscale characterisation of fracture patterns: A case study of the Noble Hills Range (Death Valley, CA, USA), application to geothermal reservoirs. *Geosciences* 11:280. <https://doi.org/10.3390/geosciences11070280>

14. Chabani A, Trullenque G, Klee J, Ledésert BA (2021b) Fracture spacing variability and the distribution of fracture patterns in granitic geothermal reservoir: A case study in the Noble Hills Range (Death Valley, CA, USA). *Geosciences* 11:520. <https://doi.org/10.3390/geosciences11120520>
15. Chapelet M, Dezayes C, Dewez T (2020) Characterization of fracture network based on photogrammetry. In *Proceedings World Geothermal Congress 2020+1*, Reykjavik, Iceland, April-October 2021.
16. Chapman FM, Miranda MM, Soucy La Roche R, Raymond J. Fracture network analysis in the Duke River area, southwestern Yukon. Submitted to *Yukon Exploration Geology*.
17. Clark T, Wares R (2004) Synthèse lithotectonique et métallogénique de l'Orogène du Nouveau-Québec (Fosse du Labrador). MERN, Québec (QC), Canada
18. Colica E, D'Amico S, Iannucci R, Martino S, Gauci A, Galone L, Galea P, Paciello A (2021) Using unmanned aerial vehicle photogrammetry for digital geological surveys: case study of Selmun promontory, northern Malta. *Environmental Earth Sciences* 80:551. <https://doi.org/10.1007/s12665-021-09846-6>
19. Corrigan D, Hajnal Z, Németh B, Lucas SB (2005) Tectonic framework of a Paleoproterozoic arc-continent to continent-continent collisional zone, Trans-Hudson Orogen, from geological and seismic reflection studies. *Canadian Journal of Earth Sciences* 42:421-434. <https://doi.org/10.1139/e05-025>
20. Corrigan D, Pehrsson S, Wodicka N, de Kemp E (2009) The Palaeoproterozoic Trans-Hudson Orogen: a prototype of modern accretionary processes. *Geological Society* 327:457-479.
21. Corrigan D, Wodicka N, McFarlane C, Lafrance I, van Rooyen D, Bandyayera D, Bilodeau C (2018) Lithotectonic framework of the Core Zone, Southeastern Churchill Province, Canada. *Geoscience Canada* 45:1-24. <https://doi.org/10.12789/geocanj.2018.45.128>
22. Darbyshire FA, Bastow ID, Petrescu L, Gilligan A, Thompson DA (2017) A tale of two orogens: Crustal processes in the Proterozoic Trans-Hudson and Grenville Orogens, eastern Canada. *Tectonics* 36:1633-1659. <https://doi.org/10.1002/2017TC004479>
23. Davis DW, Moukhsil A, Lafrance I, Hammouche H, Goutier J, Pilote P, Takam FT (2015) Datations U-Pb dans les provinces du Supérieur, de Churchill et de Grenville effectuées au JSGL en 2012-2013. MERN, Québec (QC), Canada
24. Dieterich JH (1992) Earthquake nucleation on faults with rate-and state-dependent strength. *Tectonophysics* 211:115-134. [https://doi.org/10.1016/0040-1951\(92\)90055-B](https://doi.org/10.1016/0040-1951(92)90055-B)
25. Eshelby JD (1957) The determination of the elastic field of an ellipsoidal inclusion, related problems. *Proceedings of the Royal Society A Mathematical, Physical Engineering Sciences* 241.
26. Espejel RL, Alves TM, Blenkinsop TG (2020) Multi-scale fracture network characterisation on carbonate platforms. *Journal of Structural Geology* 140:104160. <https://doi.org/10.1016/j.jsg.2020.104160>
27. ESRI (2021) How to: Batch calculate line direction using the Field Calculator. <https://support.esri.com/en/technical-article/000015375>. Accessed on 09 September 2022.

28. Fisher JE, Shakoor A, Watts CF (2014) Comparing discontinuity orientation data collected by terrestrial LiDAR and transit compass methods. *Engineering Geology* 181:78-92. <https://doi.org/10.1016/j.enggeo.2014.08.014>
29. Frey M, Bossennec C, Seib L, Bär K, Schill E, Sass I (2022) Interdisciplinary fracture network characterization in the crystalline basement: a case study from the Southern Odenwald, SW Germany. *Solid Earth* 13:935-955. <https://doi.org/10.5194/se-13-935-2022>
30. GCan (2022) Pan-Canadian Framework on Clean Growth and Climate Change. <https://www.canada.ca/en/services/environment/weather/climatechange/pan-canadian-framework.html>. Accessed on 07 September 2022
31. Genter A, Evans K, Cuenot N, Fritsch D, Sanjuan B (2010) Contribution of the exploration of deep crystalline fractured reservoir of Soultz to the knowledge of enhanced geothermal systems (EGS). *Comptes Rendus Geoscience* 342:502-516. <https://doi.org/10.1016/j.crte.2010.01.006>
32. Gillespie PA, Howard CB, Walsh JJ, Watterson J (1993) Measurement and characterisation of spatial distributions of fractures. *Tectonophysics* 226:113-141. [https://doi.org/10.1016/0040-1951\(93\)90114-Y](https://doi.org/10.1016/0040-1951(93)90114-Y)
33. Giordano N, Raymond J (2019) Alternative and sustainable heat production for drinking water needs in a subarctic climate (Nunavik, Canada): Borehole thermal energy storage to reduce fossil fuel dependency in off-grid communities. *Applied Energy* 252:113463. <https://doi.org/10.1016/j.apenergy.2019.113463>
34. Glaas C, Vidal J, Genter A (2021) Structural characterization of naturally fractured geothermal reservoirs in the central Upper Rhine Graben. *Journal of Structural Geology* 148:104370. <https://doi.org/10.1016/j.jsg.2021.104370>
35. Golden Software (2022) Grapher. <https://www.goldensoftware.com/products/grapher>. Accessed on 09 September 2022.
36. Goulet N (1995) Études structurales, stratigraphiques et géochronologiques de la partie nord de la Fosse du Labrador. MERN, Québec (QC), Canada.
37. Grasby SE, Allen DM, Bell S, Chen Z, Ferguson G, Jessop A, Kelman M, Ko M, Majorowicz J, Moore M, Raymond J, Therrien R (2012) Geothermal Energy Resource Potential of Canada, Open File 6914; Geological Survey of Canada: Calgary (AB), Canada
38. Guerriero V, Vitale S, Ciarcia S, Mazzoli S (2011) Improved statistical multi-scale analysis of fractured reservoir analogues. *Tectonophysics* 504:14-24. <https://doi.org/10.1016/j.tecto.2011.01.003>
39. Gunawan E, Giordano N, Jensson P, Newson J, Raymond J (2020) Alternative heating systems for northern remote communities: Techno-economic analysis of ground-coupled heat pumps in Kuujuaq, Nunavik, Canada. *Renewable Energy* 147:1540-1553. <https://doi.org/10.1016/j.renene.2019.09.039>
40. Gutierrez M, Youn D-J (2015) Effects of fracture distribution and length scale on the equivalent continuum elastic compliance of fractured rock masses. *Journal of Rock Mechanics and Geotechnical Engineering* 2015, 7, 626-637. <https://doi.org/10.1016/j.jrmge.2015.07.006>

41. Hall J, Loudon KE, Funck T, Deemer S (2002) Geophysical characteristics of the continental crust along the Lithoprobe Eastern Canadian Shield Onshore-Offshore Transect (ECSOOT): a review. *Canadian Journal of Earth Sciences* 39:569-587. <https://doi.org/10.1139/e02-005>
42. Hammer PTC, Clowes RM, Cook FA, van der Velden AJ, Vasudevan K (2010) The lithoprobe transcontinental lithospheric cross sections: imaging the internal structure of the North American continent. *Canadian Journal of Earth Sciences* 47. <https://doi.org/10.1139/E10-036>
43. Hamzhepour H, Pazoki S, Khazaei M, Sahimi M (2021) Dependence of percolation and flow properties of fracture networks on the morphology. *Physica A: Statistical Mechanics and its Applications* 584:126361. <https://doi.org/10.1016/j.physa.2021.126361>
44. Hardebol NJ, Maier C, Nick H, Geiger S, Bertotti G, Boro H (2015) Multiscale fracture network characterization and impact on flow: A case study on the Latemar carbonate platform. *JGR Solid Earth* 120: 8197-8222. <https://doi.org/10.1002/2015JB011879>
45. Hoffman PF (1988) United plates of America, the birth of a craton: Early Proterozoic assembly and growth of Laurentia. *Annual Review of Earth and Planetary Sciences* 16:543-603. <https://doi.org/10.1146/annurev.ea.16.050188.002551>
46. ISRM (1978) Suggested methods for the quantitative description of discontinuities in rock masses. *International Journal of Rock Mechanics and Mining Sciences & Geomechanics Abstracts* 15:319-368.
47. James DT, Connelly JN, Wasteneys HA, Kilfoil GJ (1996) Paleoproterozoic lithotectonic divisions of the southeastern Churchill Province, western Labrador. *Canadian Journal of Earth Sciences* 33.
48. Jing Z, Willis-Richards J, Watanabe K, Hashida T (2000) A three-dimensional stochastic rock mechanics model of engineered geothermal systems in fractured crystalline rocks. *Journal of Geophysical Research* 105:23,663-23,679. <https://doi.org/10.1029/2000JB900202>
49. Kanzari I (2019) Évaluation du potentiel des pompes à chaleur géothermique pour la communauté nordique de Kuujuaq. Master thesis, INRS, Quebec (QC), Canada
50. Kong D, Saroglou C, Wu F, Sha P, Li B (2021) Development and application of UAV-SfM photogrammetry for quantitative characterization of rock mass discontinuities. *International Journal of Rock Mechanics and Mining Sciences* 141:104729. <https://doi.org/10.1016/j.ijrmms.2021.104729>
51. Kunkel T, Ghomsei M, Ellis R (2012) Geothermal energy as an indigenous alternative energy source in BC. *Journal of Ecosystems & Management* 13.
52. Lafrance I, Vanier M-A, Charette B (2020) Baleine lithotectonic domain, Southeastern Churchill Province, Nunavik, Quebec, Canada: Geological synthesis. https://gq.mines.gouv.qc.ca/bulletins-geologiques_en/churchill_en/baleine_en/. Accessed on 09 September 2022
53. Ledésert B, Hebert R, Genter A, Bartier D, Clauer N, Grall C (2010) Fractures, hydrothermal alterations and permeability in the Soultz Enhanced Geothermal System. *Comptes Rendus Geoscience* 342:607-615. <https://doi.org/10.1016/j.crte.2009.09.011>

54. Lei Q, Latham J-P, Tsang C-F (2017) The use of discrete fracture networks for modelling coupled geomechanical and hydrological behaviour of fractured rocks. *Computers and Geotechnics* 85:151-176. <https://doi.org/10.1016/j.compgeo.2016.12.024>
55. Mahbaz SB, Dehghani-Sanij AR, Dusseault MB, Nathwani JS (2020) Enhanced and integrated geothermal systems for sustainable development of Canada's northern communities. *Sustainable Energy Technologies and Assessments* 37:100565. <https://doi.org/10.1016/j.seta.2019.100565>
56. Majorowicz J, Grasby SE (2014) Geothermal energy for northern Canada: Is it economical?. *Natural Resources Research* 23:159-173. <https://doi.org/10.1007/s11053-013-9199-3>
57. Majorowicz JA, Minea V (2015) Shallow and deep geothermal energy potential in low heat flow/cold climate environment: northern Quebec, Canada, case study. *Environmental Earth Sciences* 74:5233-5244. <https://doi.org/10.1007/s12665-015-4533-1>
58. Manzocchi T (2002) The connectivity of two-dimensional networks of spatially correlated fractures. *Water Resources Research* 38. <https://doi.org/10.1029/2000WR000180>
59. McFarlan A (2018) Techno-economic assessment of pathways for electricity generation in northern remote communities in Canada using methanol and dimethyl ether to replace diesel. *Renewable and Sustainable Energy Reviews* 90:863-876. <https://doi.org/10.1016/j.rser.2018.03.076>
60. MERN (2020) Churchill Province. https://gq.mines.gouv.qc.ca/lexique-stratigraphique/province-de-churchill_en/. Accessed on 09 September 2022.
61. MERN (2020) Pingiajjulik fault. https://gq.mines.gouv.qc.ca/lexique-structural/faille-de-pingiajjulik_en/. Accessed on 09 September 2022.
62. MERN (2019) SIGÉOM. https://sigeom.mines.gouv.qc.ca/signet/classes/I1108_afchCarteIntr. Accessed on 09 September 2022.
63. Miranda MM, Raymond J, Willis-Richards J, Dezayes C (2021) Are engineered geothermal energy systems a viable solution for arctic off-grid communities? A techno-economic study. *Water* 13:3526. <https://doi.org/10.3390/w13243526>
64. Miranda MM, Raymond J (2022) Assessing Kuujjuaq's (Nunavik, Canada) deep geothermal energy potential, Rapport de recherche R2109. INRS, Quebec (QC), Canada
65. Moeck IS (2014) Catalog of geothermal play types based on geologic controls. *Renewable and Sustainable Energy Reviews* 37:867-882. <https://doi.org/10.1016/j.rser.2014.05.032>
66. Moorhead J (1989) Stratigraphy, structure and metamorphism of the Renai basement gneiss body and the adjacent cover succession in the western hinterland zone of the northern Labrador Trough, west of Kuujjuaq, northern Quebec. Master thesis, McGill University, Montreal (QC), Canada.
67. Perreault S, Hynes A (1990) Tectonic evolution of the Kuujjuaq terrane, New Quebec Orogen. *Geoscience Canada* 17.
68. Poirier GG (1989) Structure and metamorphism of the eastern boundary of the Labrador Trough near Kuujjuaq, Québec, and its tectonic implications. Master thesis, McGill University, Montreal (QC), Canada.

69. Poirier G, Perreault S, Hynes A, Lewry JF, Stauffer MR (1990) Nature of the eastern boundary of the Labrador Trough near Kuujuaq, Quebec. In *The Early Proterozoic Trans-Hudson Orogen of North America: Lithotectonic Correlations and Evolution*; Lewry, J.F., Stauffer, M.R., Eds.; Geological Association of Canada: St. John's (NL), Canada; 37, pp. 397-412.
70. Pollack A, Horne R, Mukerji T (2021) What are the challenges in developing enhanced geothermal systems (EGS)? Observations from 64 EGS sites. In *Proceedings of the World Geothermal Congress 2020+1*, Reykjavik, Iceland, April-October 2021.
71. Quitaras MRD (2020) Holistic and integrated energy system optimization in reducing diesel dependence of Canadian remote Arctic communities. PhD thesis, University of Victoria, Victoria (BC), Canada
72. Ranjitkar G, Huang J, Tung T (2006) Application of micro-hydropower technology for remote regions. In *2006 IEEE EIC Climate Change Conference*, Ottawa (ON), Canada, 10-12 May 2006.
73. Reinecker J, Gutmanis J, Foxford A, Cotton L, Dalby C, Law R (2021) Geothermal exploration and reservoir modelling of the United Downs deep geothermal project, Cornwall (UK). *Geothermics* 97: 102226. <https://doi.org/10.1016/j.geothermics.2021.102226>
74. Renshaw CE (1999) Connectivity of joint networks with power law length distributions. *Water Resources Research* 35:2661-2670. <https://doi.org/10.1029/1999WR900170>
75. Richards HG, Parker RH, Green ASP, Jones RH, Nicholls JDM, Nicol DAC, Randall MM, Richards S, Stewart RC, Willis-Richards J (1994) The performance and characteristics of the experimental hot dry rock geothermal reservoir at Rosemanowes, Cornwall (1985-1988). *Geothermics* 23:73-109. [https://doi.org/10.1016/0375-6505\(94\)90032-9](https://doi.org/10.1016/0375-6505(94)90032-9)
76. Salvini R, Mastroiocco G, Seddaiu, M, Rossi D, Vanneschi C (2017) The use of an unmanned aerial vehicle for fracture mapping within a marble quarry (Carrara, Italy): photogrammetry and discrete fracture network modelling. *Geomatics, Natural Hazards and Risk* 8:34-52. <https://doi.org/10.1080/19475705.2016.1199053>
77. Sanderson DJ, Peacock DCP (2019) Line sampling of fracture swarms and corridors. *Journal of Structural Geology* 122:27-37. <https://doi.org/10.1016/j.jsg.2019.02.006>
78. Simard M, Lafrance I, Hammouche H, Legoux C (2013) Géologie de la région de Kuujuaq et de la baie d'Ungava (SNRC 24J, 24K). MERN, Québec (QC), Canada.
79. Stephen JD, Mabee WE, Pribowo A, Pledger S, Hart R, Tellio S, Bull GQ (2016) Biomass for residential and commercial heating in a remote Canadian aboriginal community. *Renewable Energy* 86:563-575. <https://doi.org/10.1016/j.renene.2015.08.048>
80. Thompson S, Duggirala B (2009) The feasibility of renewable energies at an off-grid community in Canada. *Renewable and Sustainable Energy Reviews* 13:2740-2745. <https://doi.org/10.1016/j.rser.2009.06.027>
81. Tóth E, Hrabovszki E, Schubert F, Tóth TM (2022) Discrete fracture network (DFN) modelling of a high-level radioactive waste repository host rock and the effects on its hydrogeological behaviour. *Journal of Structural Geology* 156:104556. <https://doi.org/10.1016/j.jsg.2022.104556>

82. Tran NH (2007) Fracture orientation characterization: Minimizing statistical modelling errors. *Computational Statistics & Data Analysis* 51:3187-3196. <https://doi.org/10.1016/j.csda.2006.10.024>
83. Vega B, Kovscek AR (2022) Fractal characterization of multimodal, multiscale images of shale rock fracture networks. *Energies* 15:1012. <https://doi.org/10.3390/en15031012>
84. Walsh W (2013) Geothermal resource assessment of the Clarke Lake Gas Field, Fort Nelson, British Columbia. *Bulletin of Canadian Petroleum Geology* 61:241-251. <https://doi.org/10.2113/gscpgbull.61.3.241>
85. Wardle RJ, Ryan B, Ermanovics I (1990) The eastern Churchill Province, Torngat and New Quebec orogens: An overview. *Geoscience Canada* 17.
86. Wardle RJ, van Kranendonk MJ (1996) The Palaeoproterozoic Southeastern Churchill Province of Labrador-Quebec, Canada: orogenic development as a consequence of oblique collision and indentation. *Geological Society* 112:137-153. <https://doi.org/10.1144/GSL.SP1996.112.01.0>
87. Wardle RJ, James DT, Scott DJ, Hall J (2002) The southeastern Churchill Province: synthesis of a Palaeoproterozoic transpressional orogen. *Canadian Journal of Earth Sciences* 39, 639-663. <https://doi.org/10.1139/e02-004>
88. Watkins H, Bond CE, Healy D, Butler RWH (2015) Appraisal of fracture sampling methods and a new workflow to characterise heterogeneous fracture networks at outcrop. *Journal of Structural Geology* 72:67-82. <https://doi.org/10.1016/j.jsg.2015.02.001>
89. Whitmeyer SJ, Karlstrom KE (2007) Tectonic model for the Proterozoic growth of North America. *Geosphere* 3:220-259. <https://doi.org/10.1130/GES00055.1>
90. Willis-Richards J, Watanabe K, Takahashi H (1996) Progress toward a stochastic rock mechanics model of engineered geothermal systems. *Journal of Geophysical Research* 101:17,481-17,496. <https://doi.org/10.1029/96JB00882>
91. Yan C, Rousse D, Glaus M (2019) Multi-criteria decision analysis ranking alternative heating systems for remote communities in Nunavik. *Journal of Cleaner Production* 208:1488-1497. <https://doi.org/10.1016/j.jclepro.2018.10.104>
92. Zeeb C, Gomez-Rivas E, Bons PD, Blum P (2013a) Evaluation of sampling methods for fracture network characterization using outcrops. *AAPG Bulletin* 97:1545-1566.
93. Zeeb C, Gomez-Rivas E, Bons PD, Virgo S, Blum P (2013b) Fracture network evaluation program (FraNEP): A software for analyzing 2D fracture trace-line maps. *Computers & Geosciences* 60:11-22. <https://doi.org/10.1016/j.cageo.2013.04.027>

Figures

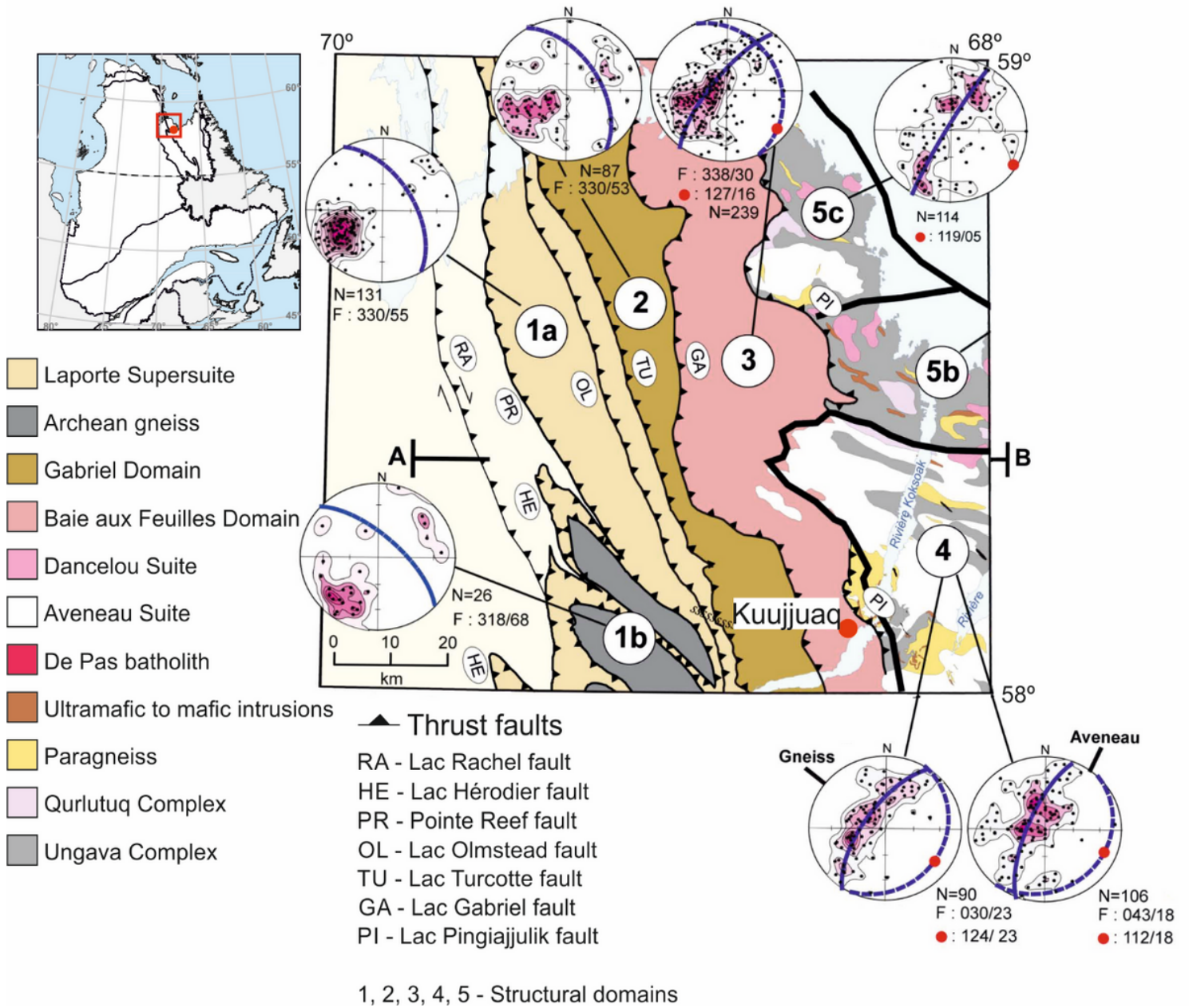


Figure 1

Structural domains and structural analysis of the southwestern Ungava Bay region. The reader is referred to the original structural map for further details (after Simard et al., 2013).

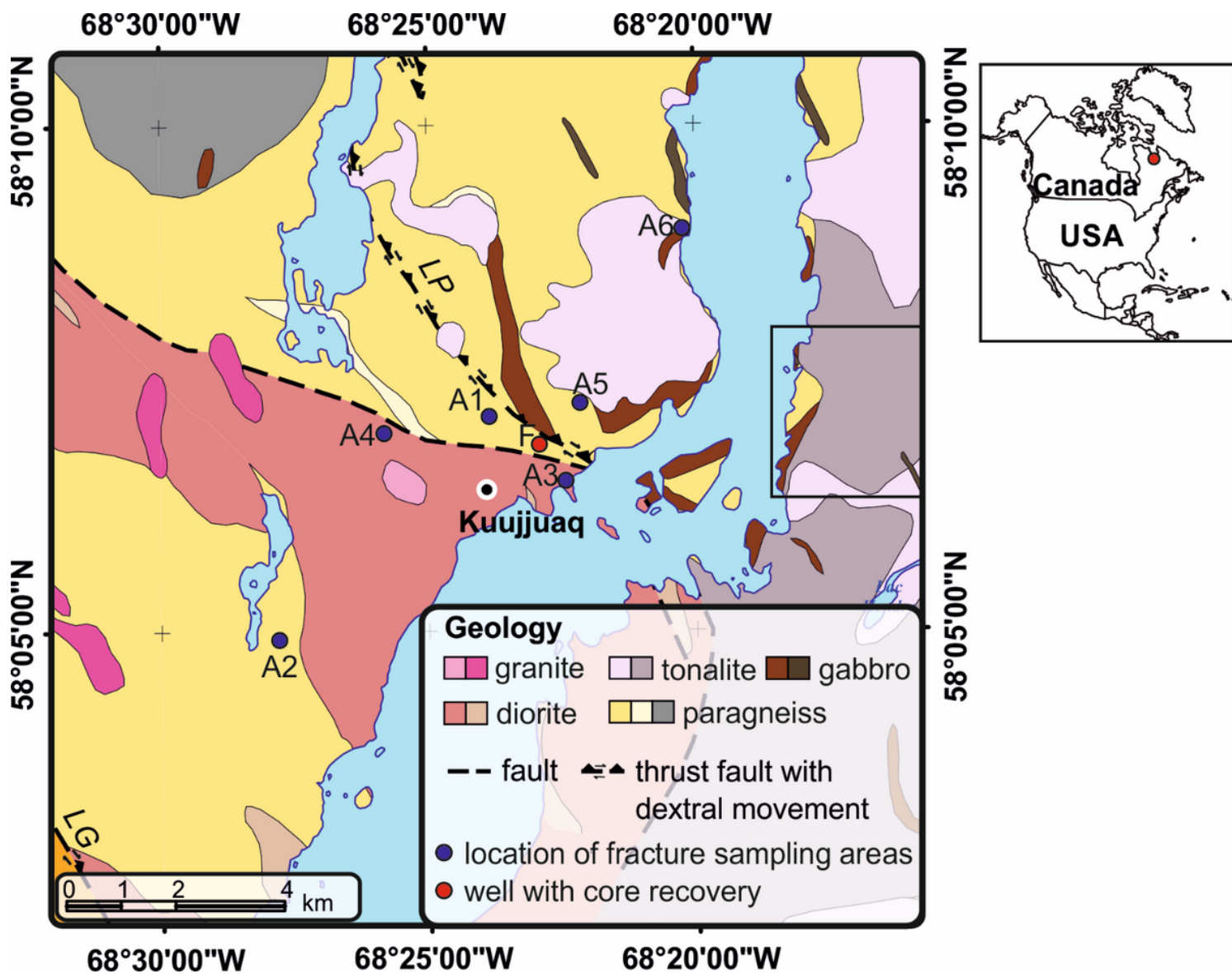


Figure 2

Geology of Kuujuaq (adapted from MERN, 2019). Black square on the geological map indicates the location of satellite image for structural lineament interpretation. LP – Lac Pingiajjulik fault, LG – Lac Gabriel fault, F – Forum well.

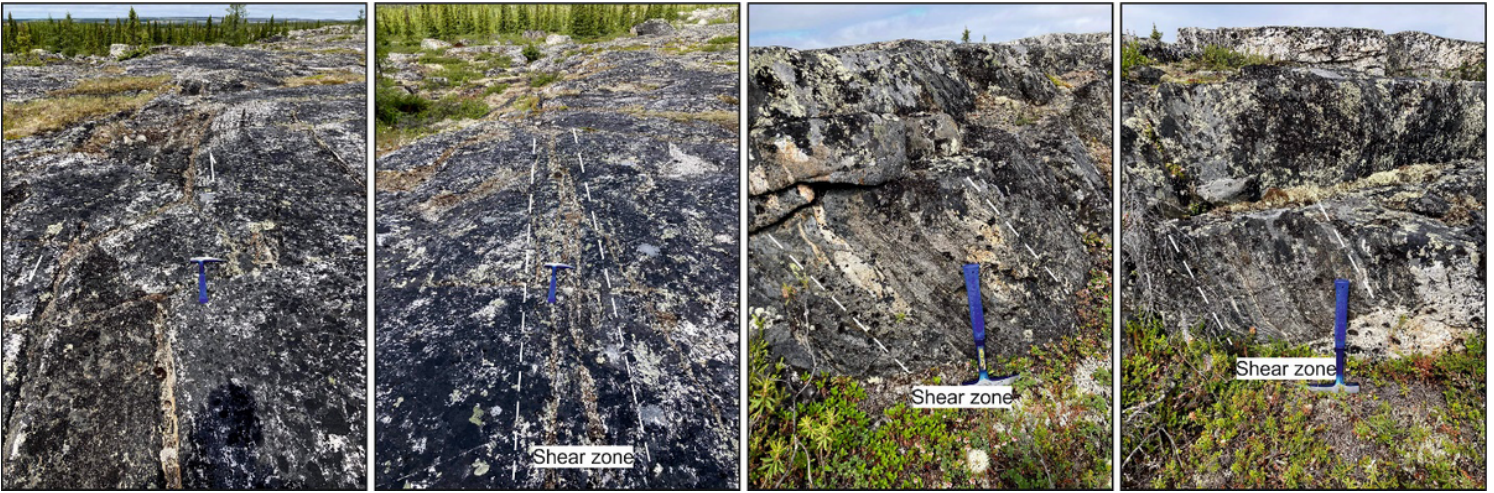


Figure 3

Mylonitic foliation suggesting the presence of the Lac Pingiajjulik fault in horizontal (left-hand side) and vertical (right-hand side) surfaces.

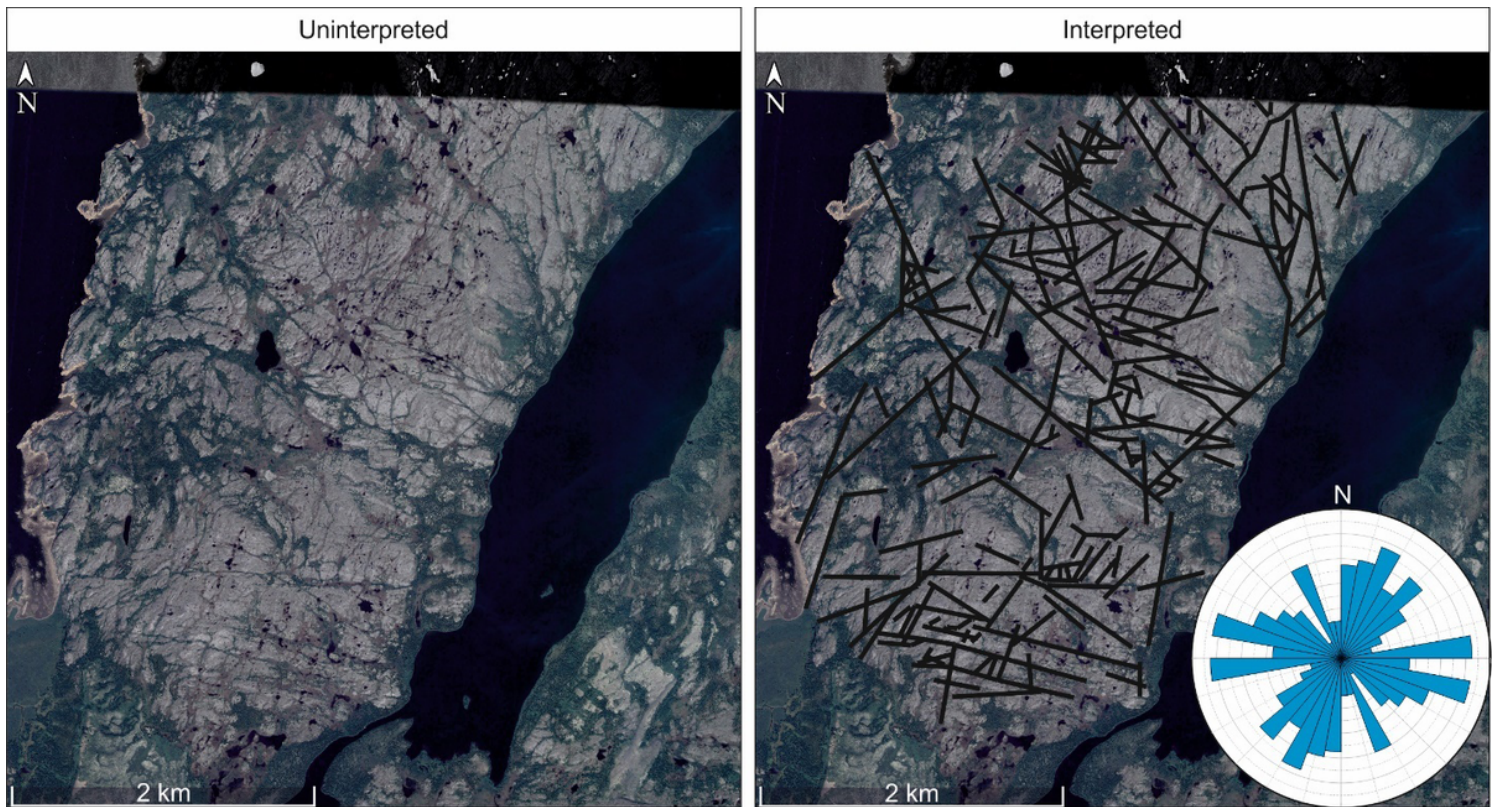


Figure 4

Google Earth satellite image and rose diagram produced from structural lineament interpretation. The reader is referred to Figure 2 for geographical location of the outcrop. The rose diagram was built with Grapher (Golden Software, 2022).

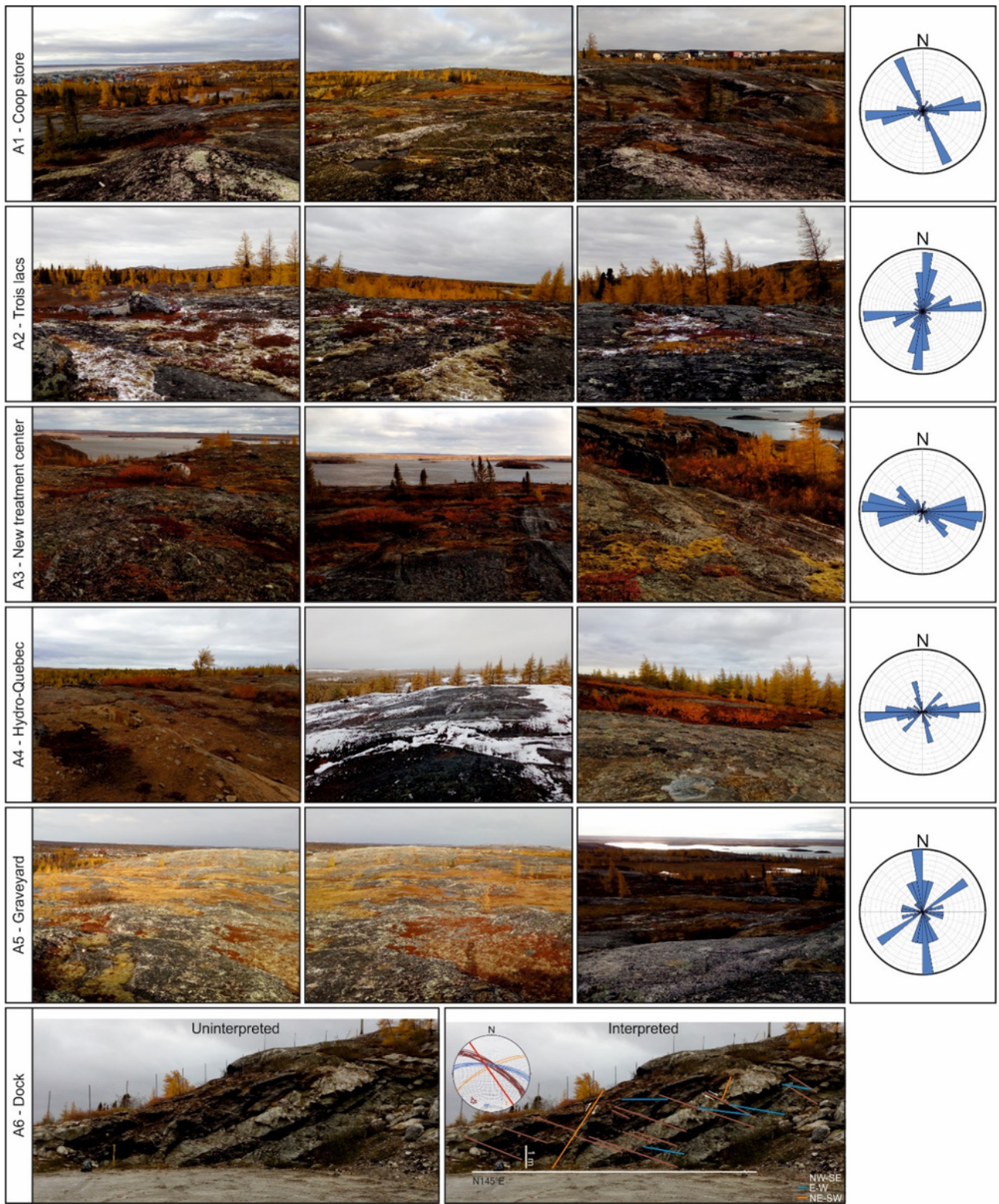
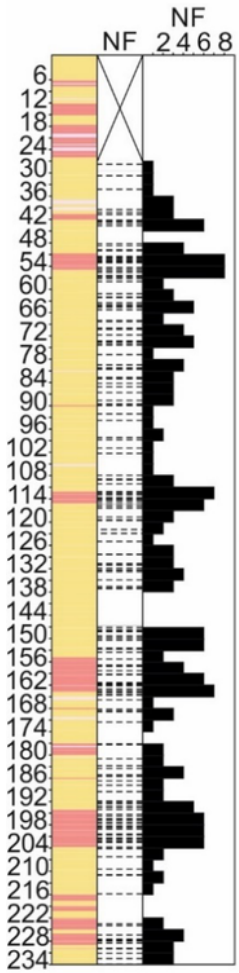


Figure 5

Representative photos of the different fracture sampling areas analyzed and rose diagrams and stereonet produced from fracture interpretation. Red line in the stereonet indicates the outcrop orientation. The stereonet canvas was built with Stereonet version 11.3.7 (Allmendinger, 2021). The reader is referred to Figure 2 for geographical location of the sampling areas.

Paragneiss samples



Diorite/gabbro samples



Possible natural fractures interpreted

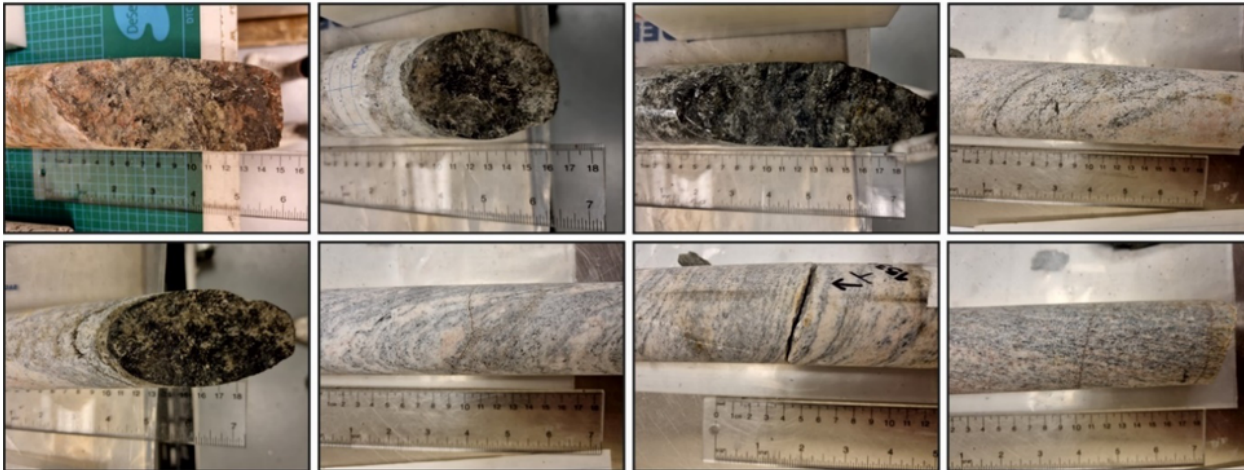


Figure 6

Graphical well log and representative photos of the lithologies encountered and natural fractures interpreted. NF – possible natural fractures displayed in stick plot and absolute frequency histogram for 3 m interval. The reader is referred to Figure 2 for geographical location of the well.

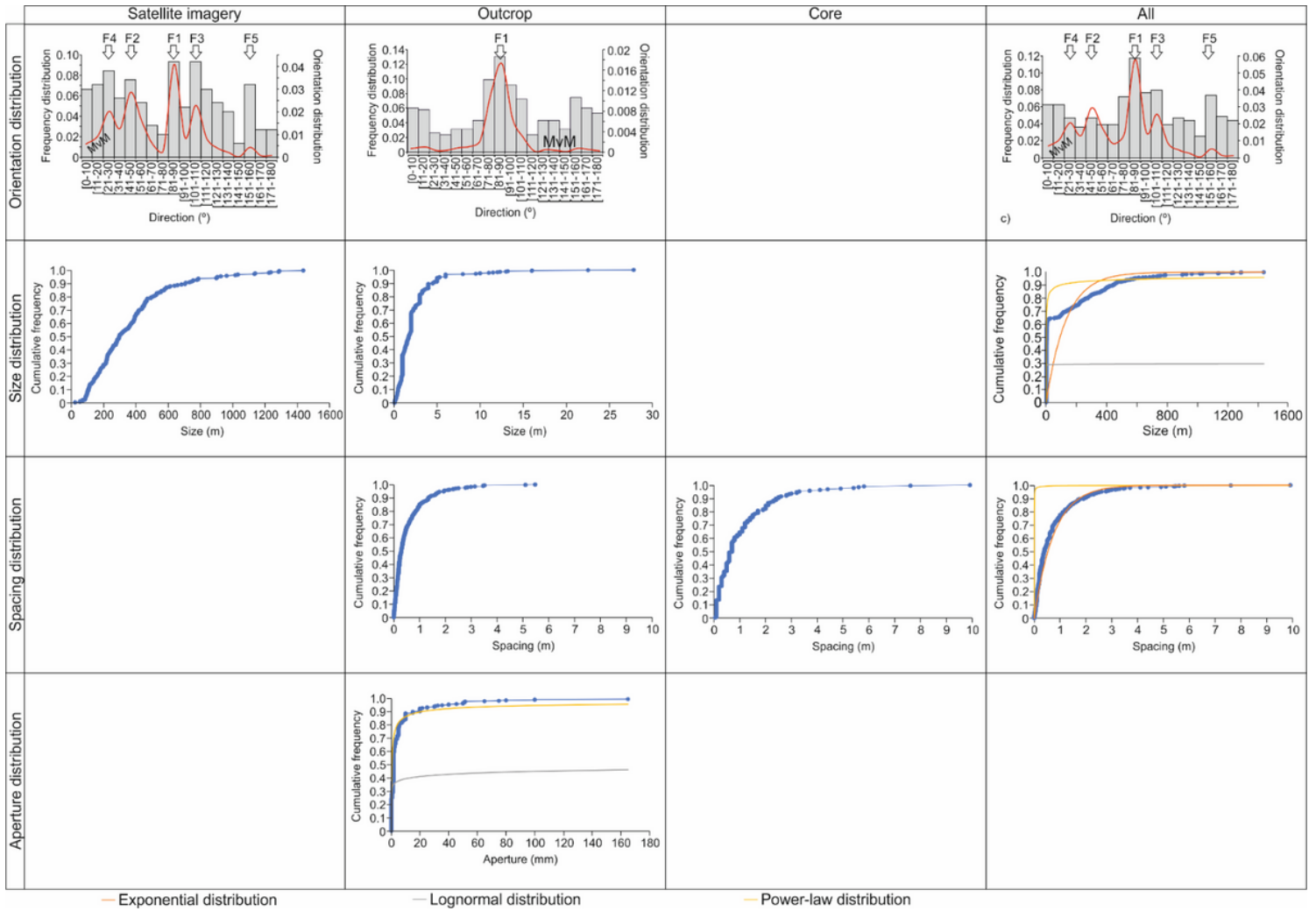


Figure 7

Statistical analysis of the geometrical attributes.

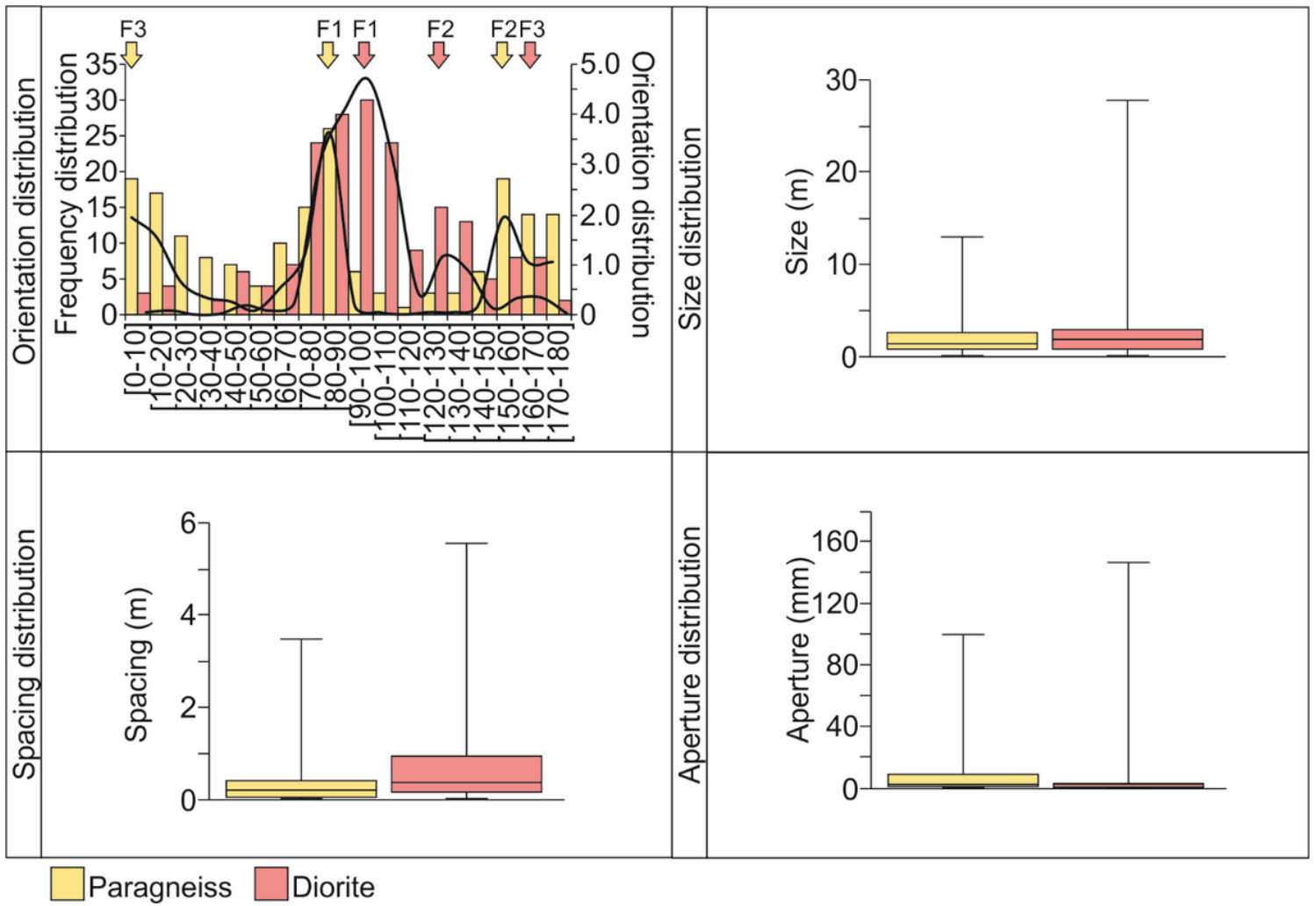


Figure 8

Influence of lithology on the geometrical attributes of fractures.

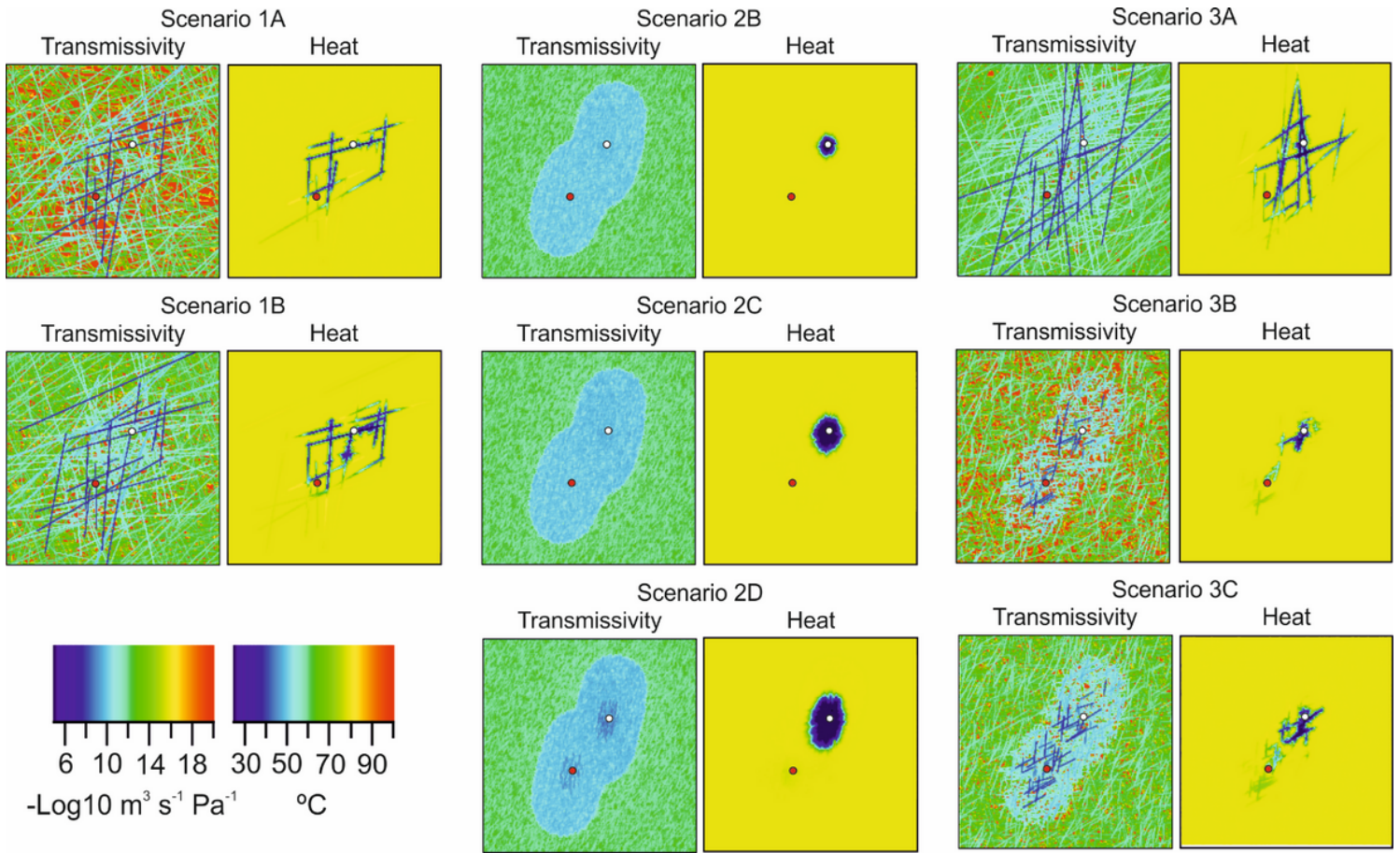


Figure 9

Top view slice at the center of the model illustrating the influence of fracture size, fracture frequency and fluid stimulation and circulation pressure on the development of an engineered geothermal system. White dot – injection well, red dot – production well.

Supplementary Files

This is a list of supplementary files associated with this preprint. Click to download.

- [Appendix.docx](#)